

Improving the energy yield of plasma-based NO_x synthesis with *in situ* adsorption

Supporting information

Kevin H. R. Rouwenhorst^{1,2,3*}, Sybe Tabak¹, Leon Lefferts^{1*}

¹ Catalytic Processes & Materials, MESA+ Institute for Nanotechnology, University of Twente, P.O. Box 217, 7500 AE Enschede (The Netherlands)

² Ammonia Energy Association, 77 Sands Street, 6th Floor, Brooklyn, NY 11201 (United States of America)

³ Koolen Industries, Europalaan 202, 7559 SC Hengelo (The Netherlands)

* Corresponding Authors:

Kevin Rouwenhorst: k.h.r.rouwenhorst@utwente.nl

Leon Lefferts: l.lefferts@utwente.nl

Contents

Supporting information	1
S1 Sorbent preparation & characterization results	2
S1.1 Materials	2
S1.2 Sorbent preparation	2
S2.3 Sorbent characterization	2
S2 Experimental section	3
S2.1 Experimental set-up.....	3
S2.3 Plasma characterization.....	4
S3 Experimental results	4
S3.1 Surface adsorbed species	4
S3.2 Energy cost for plasma-chemical NO _x synthesis & MgO regeneration.....	5
S3.3 Selectivity NO & NO ₂	6
References	7

Number of Figures: 6

Number of Tables: 0

S1 Sorbent preparation & characterization results

The alkaline earth metal oxide MgO was used as sorbent because of its capacity to adsorb NO_x [1]. As compared to BaO and SrO, MgO is easier to handle. As compared to CaO, MgO is more stable under ambient conditions, not forming stable bulk carbonates.

S1.1 Materials

Magnesium oxide powder (MgO, >97% purity grade) was purchased from Merck. N_2 and O_2 with a purity grade of 99.999% were purchased from Linde, and water traces were removed using Agilent gas clean purification systems. A gas mixture of 2 vol.% NO_2 in 10 vol.% O_2 and 88 vol.% N_2 balance gas was purchased from Linde. All materials were used as received.

S1.2 Sorbent preparation

About 2 gram MgO sorbent was dried in an oven at 105°C and atmospheric pressure in air for 1 h, followed by drying in a vacuum oven at 120°C for 2 h.

The dried sorbent was calcined in a calcination oven at 20 mL min^{-1} air flow at 400°C for 2 h (heating rate $10^\circ\text{C min}^{-1}$) to remove any residual water. After calcining, the sorbent was pelletized using a press and crushed. The sieve fraction with particle sizes of $250\text{--}300\ \mu\text{m}$ was used for sorption tests. Last traces of H_2O were removed from the reactor at 550°C .

S2.3 Sorbent characterization

The total surface area and pore volume was determined by N_2 physisorption at -198°C using a Micromeritics Tristar. The samples were outgassed in vacuum at 300°C for 24 h before the analysis. The material was analyzed by XRD-LB (Line Broadening). The crystalline phases present in the material was determined by X-ray diffraction (XRD) using a Bruker D2 Phaser diffractometer equipped with a position-sensitive detector over a 2θ range between 10° and 90° using Cu $\text{K}\alpha$ radiation ($\lambda = 1.5418\ \text{\AA}$). The crystal size was found to be 28 nm.

The elemental composition was determined by x-ray fluorescence spectroscopy (XRF) using a Bruker S8 tiger, confirming the sample being MgO, with traces of Al and Ca (combined below $<1\ \text{wt.}\%$). The MgO was found to have a total surface area of $294\ \text{m}^2\ \text{g}^{-1}$ and a pore volume of $0.31\ \text{cm}^3\ \text{g}^{-1}$. The XRD profile for the MgO sample is shown in **Figure S1**, in line with literature [2]. The diffraction pattern confirms the presence of MgO, and the absence of hydroxide, carbonate, and bicarbonate.

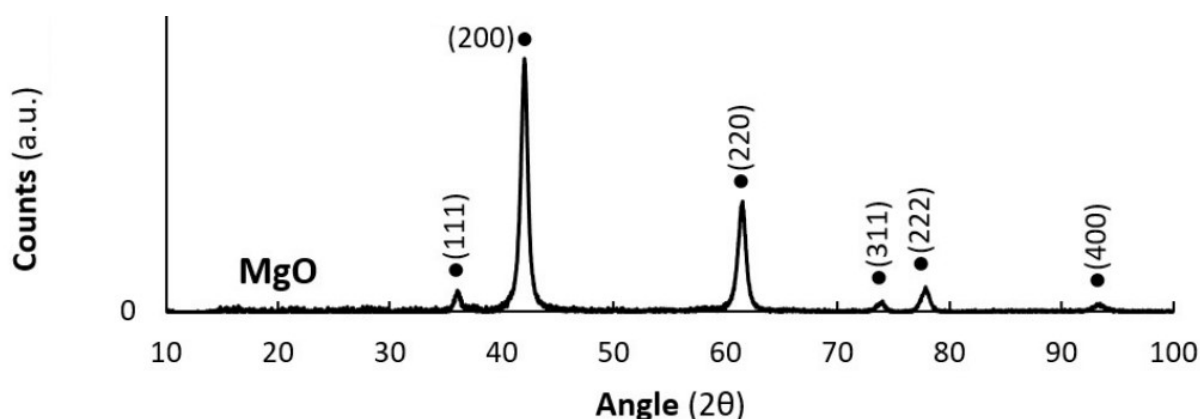


Figure S1: XRD spectrum of MgO sample. The peaks correspond well with the available JCPDS No. 87-0653 for MgO Nanoparticles.

S2 Experimental section

S2.1 Experimental set-up

A schematic representation of the experimental set-up for the tests is shown in **Figure S2**. The tests were carried out in a quartz tubular reactor with an inner diameter of 4 mm and an outer diameter of 6 mm, at atmospheric pressure. A stainless steel rod of 1 mm diameter is placed inside the reactor as the high voltage electrode. At the outside of the quartz tube, a metal tube is placed as the ground electrode. The temperature was controlled with a thermocouple connected to a heating block, which is placed around the ground electrode. Thus, the temperature is measured inside the heating block, but outside the plasma-reactor. The flowrates of the reactants were controlled with calibrated mass flow controllers (MFCs). About 300 mg of sorbent with particle size 250-300 μm was loaded in the reactor, on top of a layer of quartz wool. A spacer is placed above the catalytic bed to prevent moving of particles due to plasma-illumination and to center the high voltage electrode.

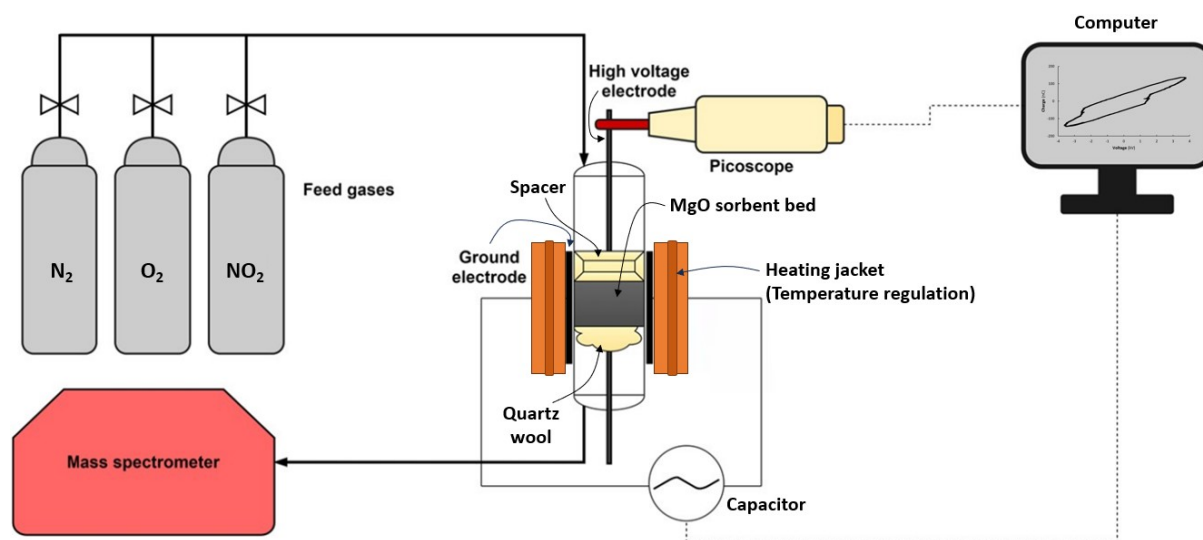


Figure S2: Schematic representation of experimental set-up. The plasma volume includes the spacer, the packed bed, and the quartz tube.

The sorbent was heated to 550°C in the reactor for 2 h in 40 mL min^{-1} N_2 flow to remove any adsorbed species prior to experiments.

A typical experiment starts with a pretreatment at 550°C for 1 h in N_2 , followed by cooling to 25°C and switching to co-feeding of N_2 and O_2 in a 1:1 ratio and a total flowrate of 20 mL min^{-1} . Then, the plasma is turned on at 6.4 W, while the other conditions remain the same. After a set amount of time, the plasma is turned off, and the flow is changed to a 10 mL min^{-1} pure N_2 flow. Subsequently, a temperature ramp is programmed at $25^\circ\text{C min}^{-1}$ up to 550°C . Afterwards, the temperature is kept at 550°C for 1 h to remove all NO_x from the MgO and the reactor is cooled down again to room temperature.

The product gases were analyzed using an on-line Pfeiffer Vacuum ThermoStarTM gas analysis system, which is a mass spectrometer (MS). The MS signals for NO_2 (30 m/e and 46 m/e) was calibrated in the range 0-2 mol.%, resulting in a linear relationship. The signals for N_2 (28 m/e), O_2 (32 m/e), NO (30 m/e), N_2O (44 m/e), and H_2O (18 m/e) were also monitored. It should be noted that both NO and NO_2 have a peak at 30 m/e. The NO_2 signal at 30 m/e is estimated based on the mass spectrum ratio vs 46 m/e [3]. See also section S3.4 for additional information on data interpretation.

S2.3 Plasma characterization

The voltage and charge were monitored with an oscilloscope, from which the power dissipated can be determined using a Lissajous figure. An example of a Lissajous figure (also termed Q-V plot) is shown in **Figure S3**. In a Q-V plot, the capacitive and discharge behaviour of a plasma is monitored. Ideally, a Lissajous figure has the shape of a parallelogram, thereby perfectly separating the capacitive and discharge regime. However, there is an indent in both the positive and negative charge cycle, as shown in **Figure S3**. This can be attributed to a discharge at the contact points of particles at an earlier stage than over the remainder of the surface [4], [5].

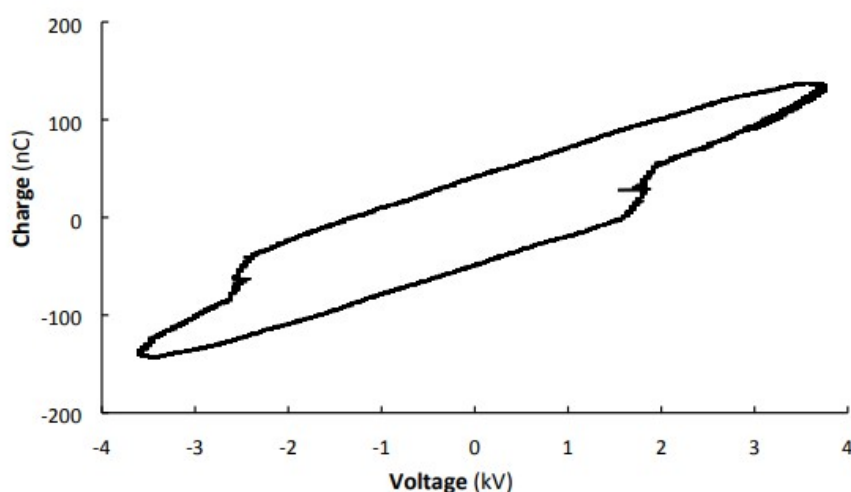


Figure S3: Lissajous figure for MgO at room temperature, $N_2:O_2=1:1$, 20 mL min^{-1} . The total power dissipated is 6.4 W.

S3 Experimental results

S3.1 Surface adsorbed species

NO only physisorbs on MgO [1], with desorption already occurring at room temperature [6]. On the other hand, NO_2 is readily adsorbed on MgO [1], [6]. This indicates that the peak for NO_x desorption at about 550°C in **Figure 2** in the main text can be attributed to desorbed NO_2 . The peak at 250°C for desorption of the $NO_{2,ads}$ species is only observed for the thermal TPD (Temperature Programmed Desorption) studies in **Figure 3** in the main text, and not for the plasma-based NO_x synthesis experiments (**Figure 2** and **Figure 3** in the main text). This can be attributed to a heating effect due to the plasma, as discussed in the main text.

NO_2 can adsorb on MgO as adsorbed NO_2 and adsorbed NO_3 [6]. It is suggested that $NO_{3,ads}$ is formed via reaction of surface adsorbed O_{ads} (not MgO lattice O) with NO_2 in gas phase [6]. Alternatively, two adsorbed $NO_{2,ads}$ species may disproportionate to $NO_{3,ads}$ and NO in the gas phase on Mg sites [6], [7].

The weakest adsorption is via $NO_{2,ads}$, which desorbs at about $125\text{-}250^\circ\text{C}$ from the MgO surface [6]. $NO_{3,ads}$ is more strongly bound to the MgO surface, and desorbs at temperatures above 400°C [6]. Thus, $NO_{3,ads}$ is the dominant surface species after exposure to the $N_2\text{-}O_2$ plasma.

To test this, the NO_2 desorption signal and the O_2 signal are shown in **Figure S4**. The observation that O_2 and NO_2 desorb simultaneously confirms the presence of an adsorbed NO_3 species, which desorbs according $2NO_{3,ads} \rightarrow 2NO_2 + O_2$.

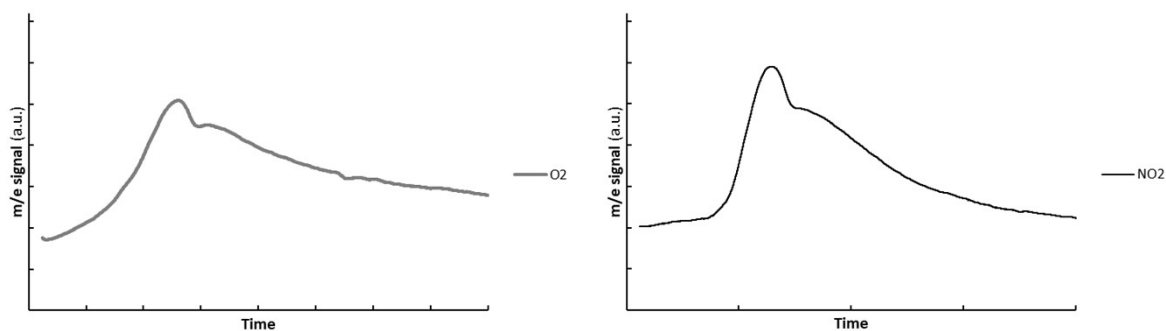


Figure S4: m/e signals for O₂ (m/e=32) [Left] and NO_x (m/e=30) [Right] during desorption after plasma-chemical NO_x synthesis with *in situ* NO_x adsorption.

S3.2 Energy cost for plasma-chemical NO_x synthesis & MgO regeneration

The energy cost of plasma-chemical NO_x synthesis with *in situ* adsorption is estimated based on the plasma power and the NO_x yield on the sorbent. The amount of NO_x adsorbed on 300 mg MgO sorbent is 0.36 mmol-NO_x after 5 minutes plasma exposure (see **Figure 3** in the main text). The plasma power during the experiments was 6.4 W. This results in an energy cost of 5.35 MJ mol-NO_x⁻¹.

The energy cost of MgO regeneration is assessed hereafter, determining whether it has a significant effect on the energy yield of plasma-chemical NO_x synthesis with *in situ* adsorption. The heat requirement for desorbing NO_x from the MgO is given by the sum of the heat required for increasing the temperature of the MgO, and the heat requirement for desorbing NO_x. It is assumed that the temperature is increased from 25°C to 550°C (ΔT=525°C), in accordance with Figure 2 in the main text. It is assumed that the gas heating can be recovered via heat integration in a process with parallel sorbent bed.

The heat capacity of MgO (C_p) at room temperature is about 37 J mol⁻¹ K⁻¹, increasing to 50 J mol⁻¹ K⁻¹ at 550°C [8]. For the calculations, the highest value is used. The NO₂ adsorption capacity, p_A, is equal to 0.05 mol-NO₂ mol-MgO⁻¹, based on the plateau value of the plasma-chemical NO_x synthesis experiments with *in situ* adsorption in **Figure 3** in the main text.

NO₃ is the dominant surface species for the *in situ* adsorption experiments, as discussed in section S3.2. The heat of adsorption of NO₂ forming NO_{3,ads} on MgO is 111 kJ mol⁻¹ [9], which desorbs according to $2 \text{NO}_{3,\text{ads}} \rightarrow 2\text{NO}_2 + \text{O}_2$.

The contribution of heating the MgO is then given by $C_p \cdot \Delta T / p_A = 50 \cdot 525 / 0.05 = 5.25 \cdot 10^5$ J mol-NO₂⁻¹ or 0.525 MJ mol-NO₂⁻¹. The contribution from the heat of adsorption is 111 kJ mol-NO₂⁻¹, or 0.111 MJ mol-NO₂⁻¹. The sum of the two contributions is 0.636 MJ mol-NO₂⁻¹. It should be noted that heating the MgO can be heat integrated when utilizing multiple beds in parallel in a TSA system, reducing the overall energy requirement.

Combining the energy consumption for the plasma reactor (5.35 MJ mol-NO_x⁻¹) and for the MgO sorbent regeneration (0.636 MJ mol-NO_x⁻¹), this results in a total energy consumption of 6.0 MJ mol-NO_x⁻¹. In any case, the energy requirement of the plasma dominated over the energy cost of desorption.

It should be noted that the lowest energy consumption reported for warm plasmas is 0.42 MJ mol-NO_x⁻¹ for NO_x concentrations of a few hundreds of ppmv [10], e.g. much lower than the current reported energy consumption. However, such low concentrations of NO_x would require a very large recycle and energy intensive separation steps, which would not be possible for commercial applications.

S3.3 Selectivity NO & NO₂

Figure S5 show the intensity of the m/e 30 and m/e 46 signals during the experiment shown in **Figure 2** in the main manuscript. During plasma illumination (minute 15 up till minute 78), the m/e 46 signal is approximately 35% of the m/e 30 signal. As shown in **Figure S6**, this agrees very well with the mass spectrum of NO₂ with an m/e 46 intensity of is 37% of the intensity at m/e 30. This indicates that the steady-state exit NO_x concentration is almost entirely NO₂, as NO has not any signal at m/e 46.

This result is different from that of Patil et al. [11], who reported approximately 35-70% NO selectivity from a 1:1 N₂:O₂ ratio at 1 L/min flow. However, it should be noted that Patil et al. reported a decrease in NO selectivity upon increasing the specific energy input (SEI) in the range 1.5-4.8 kJ L⁻¹. The current work operates with a SEI of 19.2 kJ L⁻¹. Thus, it can be expected that the NO selectivity further decreases with increasing SEI. A potential reason is the plasma heating effect previously reported in refs. [12], [13], accelerating the thermal formation of NO₂ from NO and O₂.

During the TPD experiment, starting at 80 minutes, the same ratio of m/e 30 and m/e 46 is observed and NO₂ is the dominant product. Only at the final temperatures of 550°C (beyond 100 minutes in **Figure S5**), the m/e 46 intensity drops to lower values than 35% of the m/e 30 intensity. It is possible that that this is caused by NO₂ decomposition to NO and O₂, due to the thermodynamic equilibrium of $2\text{NO} + \text{O}_2 \leftrightarrow \text{NO}_2$ shifting toward NO at elevated temperatures [14]. As shown in Figure S4, O₂ is indeed measured at elevated levels at elevated temperatures. This can in part be attributed to the desorption $2\text{NO}_{3,\text{ads}} \rightarrow 2\text{NO}_2 + \text{O}_2$ (see S3.1 and **Figure S4**). However, thermal decomposition of NO₂ to NO and O₂ cannot be excluded at elevated temperatures.

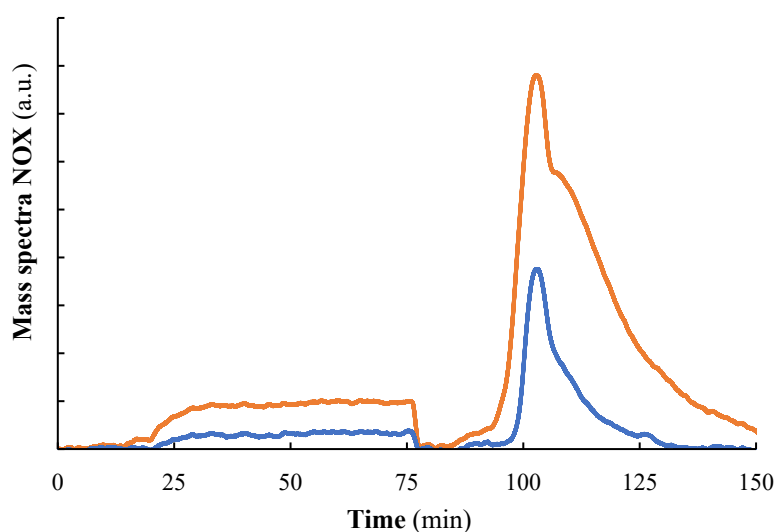


Figure S5: m/e signals for m/e 30 and m/e 46 during an *in situ* plasma experiment (the same experiment as **Figure 2** in the main manuscript).

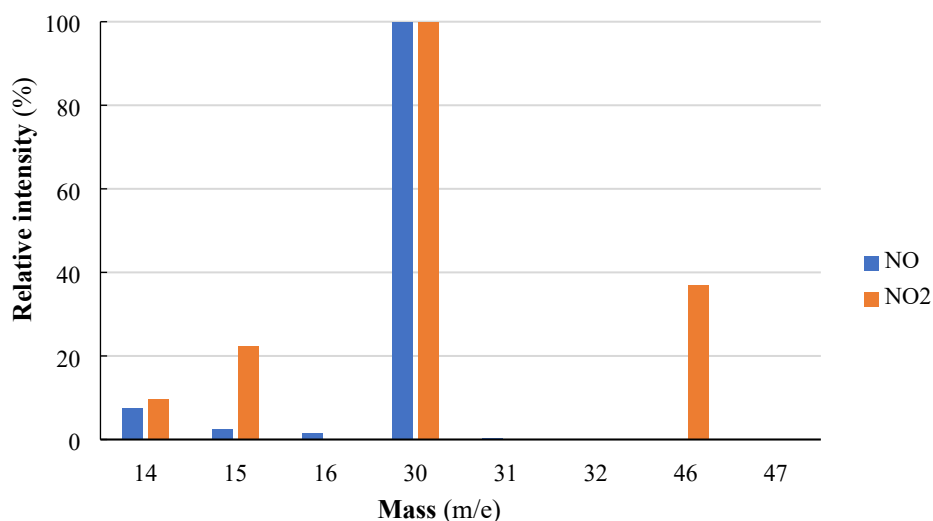


Figure S6: Mass spectra of NO and NO₂.

References

- [1] C. Verrier, J. H. Kwak, D. H. Kim, C. H. F. Peden, and J. Szanyi, "NO_x uptake on alkaline earth oxides (BaO, MgO, CaO and SrO) supported on γ -Al₂O₃," *Catal. Today*, vol. 136, no. 1–2, pp. 121–127, 2008, doi: 10.1016/j.cattod.2007.12.138.
- [2] A. Almontasser, A. Parveen, and A. Azam, "Synthesis, Characterization and antibacterial activity of Magnesium Oxide (MgO) nanoparticles," *IOP Conf. Ser. Mater. Sci. Eng.*, vol. 577, no. 1, 2019, doi: 10.1088/1757-899X/577/1/012051.
- [3] NIST, "Nitrogen dioxide," 2021. <https://webbook.nist.gov/cgi/cbook.cgi?ID=C10102440&Mask=200> (accessed Aug. 23, 2022).
- [4] A. Bogaerts, Q. Zhang, Y. Zhang, K. Van Laer, and W. Wang, "Burning questions of plasma catalysis: Answers by modeling," *Catal. Today*, vol. 337, pp. 3–14, 2019, doi: 10.1016/j.cattod.2019.04.077.
- [5] F. Herrera *et al.*, "The impact of transition metal catalysts on macroscopic dielectric barrier discharge (DBD) characteristics in an ammonia synthesis plasma catalysis reactor," *J. Phys. D. Appl. Phys.*, vol. 52, no. 22, 2019, doi: 10.1088/1361-6463/ab0c58.
- [6] J. A. Rodriguez, T. Jirsak, J. Y. Kim, J. Z. Larese, and A. Maiti, "Interaction of NO and NO₂ with MgO(1 0 0): Photoemission and density-functional studies," *Chem. Phys. Lett.*, vol. 330, no. 3–4, pp. 475–483, 2000, doi: 10.1016/S0009-2614(00)01098-8.
- [7] J. A. Rodriguez, T. Jirsak, S. Sambasivan, D. Fischer, and A. Maiti, "Chemistry of NO₂ on CeO₂ and MgO: Experimental and theoretical studies on the formation of NO₃," *J. Chem. Phys.*, vol. 112, no. 22, pp. 9929–9939, 2000, doi: 10.1063/1.481629.
- [8] NIST, "magnesium oxide," 2021. <https://webbook.nist.gov/cgi/inchi?ID=C1309484&Type=JANAFS&Plot=on> (accessed Aug. 23, 2022).
- [9] W. F. Schneider, K. C. Hass, M. Miletic, and J. L. Gland, "Dramatic Cooperative Effects in Adsorption of NO_x on MgO(001)," *J. Phys. Chem. B*, vol. 106, no. 30, pp. 7405–7413, 2002, doi: 10.1021/jp0257496.

- [10] E. Vervloessem, Y. Gorbaney, A. Nikiforov, N. De Geyter, and A. Bogaerts, "Sustainable NO_x production from air in pulsed plasma: Elucidating the chemistry behind the low energy consumption," *Green Chem.*, vol. 24, no. 2, pp. 916–929, 2022, doi: 10.1039/d1gc02762j.
- [11] B. S. Patil, N. Cherkasov, J. Lang, A. O. Ibhaddon, V. Hessel, and Q. Wang, "Low temperature plasma-catalytic NO_x synthesis in a packed DBD reactor: Effect of support materials and supported active metal oxides," *Appl. Catal. B Environ.*, vol. 194, pp. 123–133, 2016, doi: 10.1016/j.apcatb.2016.04.055.
- [12] K. H. R. Rouwenhorst, S. Mani, and L. Lefferts, "Improving the energy yield of plasma-based ammonia synthesis with in situ adsorption," *ACS Sustain. Chem. Eng.*, vol. 10, no. 6, pp. 1994–2000, 2022, doi: 10.1021/acssuschemeng.1c08467.
- [13] H.-H. Kim, Y. Teramoto, N. Negishi, and A. Ogata, "A multidisciplinary approach to understand the interactions of nonthermal plasma and catalyst: A review," *Catal. Today*, vol. 256, no. Part 1, pp. 13–22, 2015, doi: 10.1016/j.cattod.2015.04.009.
- [14] W. S. Epling, L. E. Campbell, A. Yezerets, N. W. Currier, and J. E. Parks, "Overview of the fundamental reactions and degradation mechanisms of NO_x storage/reduction catalysts," *Catal. Rev. - Sci. Eng.*, vol. 46, no. 2, pp. 163–245, 2004, doi: 10.1081/CR-200031932.